Ship Radiation and Diffraction Forces at Moderate Forward Speed

Kevin McTaggart (F)
Defence Research and Development Canada

DRDC-RDDC-2015-P168

This paper describes numerical evaluation of radiation and diffraction forces for a ship travelling in a seaway at moderate forward speed. The method was developed with the objective of providing efficient and robust force predictions in both the frequency and time domains. For evaluation of radiation and diffraction forces, it is assumed that the ship travels with quasi-steady speed and heading. Time domain computations can include nonlinearities in buoyancy and incident wave excitation forces through evaluation of pressures on the instantaneous wetted hull surface. The paper describes various aspects of the numerical implementation, and also describes limitations that have been determined through verification and validation.

KEY WORDS: Diffraction, radiation, ship motions, software, validation, verification.

INTRODUCTION

Numerical predictions of ship motions in waves are routinely used for many applications, including ship design, operational planning, and training using simulation. A very broad range of computational tools is available. Simple strip theory methods (Salvesen, Tuck, and Faltinsen 1970) can run on a desktop computer within seconds for a large number of conditions. In contrast, Reynolds-averaged Navier-Stokes (RANS) computational fluid dynamics (CFD) methods (Stern, Yang, Wang, Sadat, Hosseini, Mousaviraad, Bhushan, and Xing 2013) can require days on large-scale computers to determine motions for a ship in a single realistic seaway. For contemporary naval architecture applications, strip theory and three-dimensional

methods (Papanikolaou and Schellin 1992) assuming potential flow in the frequency domain are most commonly used. Time domain methods are becoming more commonly used, with greatly varying computational times depending on assumptions related to various factors, including water viscosity and nonlinear boundary conditions.

This paper describes prediction of ship hull forces influencing motions in waves. The assumption of potential flow greatly simplifies numerical computations and is justifiable based on the physics of ship motions in waves and validation results. Excitation forces due to incident waves are very easily evaluated. Forces arising from radiated and diffracted waves are evaluated using a three-dimensional boundary element method and the frequency domain Green function for zero forward speed (Telste and Noblesse 1986). This approach is similar to that used by Papanikolaou and Schellin (1992), and requires solution of flow terms only on the mean wetted surface of the hull. Although the Green function only fully satisfies the free surface boundary condition at zero forward ship speed, validation results indicate that reliable predictions of motions in waves can be obtained for forward speed Froude numbers $U/\sqrt{gL}$ up to 0.4, where U is forward ship speed, g is gravitational acceleration, and L is ship length between perpendiculars. Radiation and diffraction forces in the time domain are determined using force terms previously computed in the frequency domain, with time domain retardation functions evaluated using transforms given by Wehausen (1971) and Mei (1983).

OVERVIEW OF MODELLING OF SHIP HULL GEOMETRY FOR POTENTIAL FLOW COMPUTATIONS

Before considering the details of flow modelling, it is useful to consider the modelling of ship geometry that will be used for potential flow computations. In contrast to RANS CFD methods, potential flow methods can work very well with relatively coarse ship geometry meshes. Geometries for both strip theory and three-dimensional methods are considered here.

Figure 1 shows hull lines for a generic naval frigate, represented by 20 evenly spaced stations along the length of the hull. The generic frigate has length L of 120 m, waterline beam B of 14.1 m, and draft T of 4.2 m. For each hull line, the longitudinal coordinate x is constant, and the lateral and vertical coordinates y and z are functions of the non-dimensional distance v along each hull line as follows:

$$x, y \quad = \quad f(v) \text{ where } 0.0 \leq v \leq 1.0 \tag{1}$$

Figure 2 shows the same generic frigate modelled using the following 3 parametric surfaces:

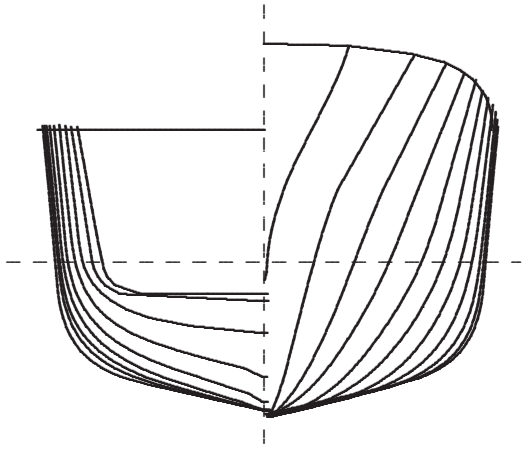

Figure 1: Hull Lines for Generic Naval Frigate

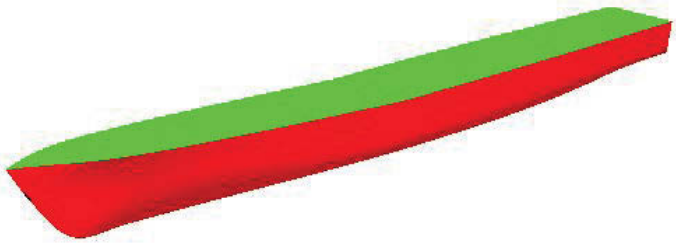

Figure 2: Parametric Surface Model for Generic Naval Frigate

1. main hull (shown in red),
2. deck (shown in green),
3. transom (hidden).

For each parametric surface, the surface coordinates are functions of the parametric variables u and v:

$$x, y, z \quad = \quad f(u, v) \text{ where } \begin{cases} 0.0 \leq u \leq 1.0 \\ 0.0 \leq v \leq 1.0 \end{cases} \tag{2}$$

In addition to parametric surfaces, trimmed parametric surfaces are commonly used to represent ship hulls, and are described by Payne and Issa (2009).

Most methods for solving ship radiation and diffraction forces discretize the hull geometry, using straight line segments for strip theory and planar panels for three-dimensional methods. Figure 3 shows a hull section discretized into straight line segments. Similarly, Figure 4 shows a hull with surfaces discretized into planar panels. For potential flow solution, strip theory typically uses of the order of 20 line segments to model a wetted hull section, while three-dimensional methods typically use of the

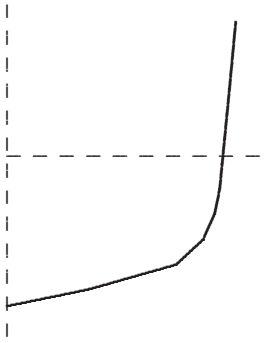

Figure 3: Discretized Midship Hull Line for Generic Naval Frigate

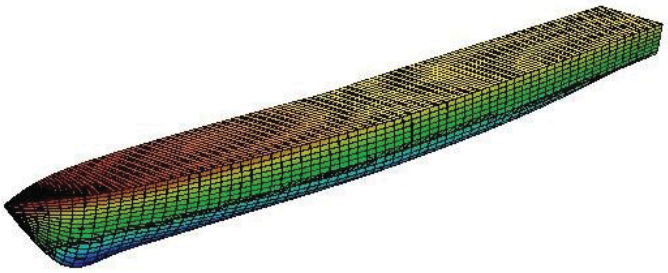

Figure 4: Planar Panel Model for Generic Naval Frigate

order of 1000 panels to model a wetted hull. The wetted hull geometry is usually determined using the full geometry and specified ship draft. Fortunately, the wetted geometry can usually be easily determined for a given ship line segment or planar panel.

Some three dimensional methods for determining radiation and diffraction forces directly use parametric surfaces rather than discretized planar panels (Lee, Letcher, Mack, Newman, Shook and Stanley 2002; Qiu, Peng, Calisal and Wang 2005). These methods can often give better accuracy than planar panel methods when solving for flow using a given number of degrees of freedom.

OVERVIEW OF SHIP RADIATION AND DIFFRACTION FORCES

The current approach evaluates ship radiation and diffraction forces in the frequency domain in a manner similar to Papanikolaou and Schellin (1992), and is described in detail in McTaggart (2002). It is assumed that the ship travels with quasi-steady forward speed and heading. The flow field and ship motions are solved using the translating earth axis system of Figure 5, which moves with the steady forward speed of the ship. For a ship with in regular waves,

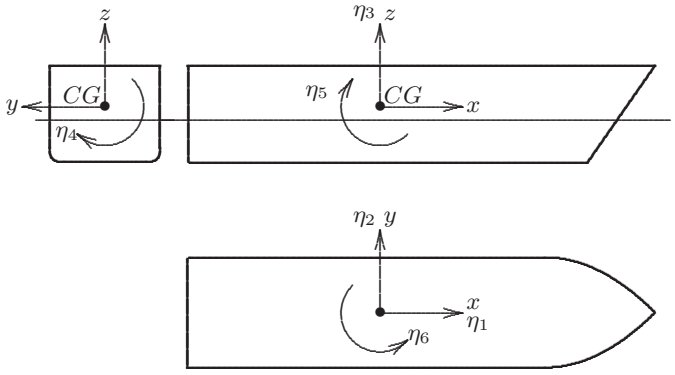

Figure 5: Translating Earth Coordinate System for Solution of Ship Motions

the velocity potential in the time domain is expressed as:

$$\Phi(\vec{x},t) = \text{Real}\left\{\left[\phi_I(\vec{x},\beta,\omega_I)+\phi_D(\vec{x},\beta,\omega_I) + \sum_{j=1}^{6}\eta_j\phi_j(\vec{x},U,\omega_e)\right] e^{i\omega_e t}\right\} \quad (3)$$

where Φ is total velocity potential, $\vec{x}$ is location, t is time, Real $\{\ldots\}$ denotes the real part of the term in brackets, ϕ_I is incident wave velocity potential, β is relative sea direction, ω_I is incident wave frequency, ϕ_D is diffracted wave velocity potential, η_j is the complex motion amplitude for mode j, ϕ_j is radiation potential for mode j, and U is steady ship forward speed. The wave encounter frequency ω_e is given by:

$$\omega_e = |\omega_I - k_I\, U\, \cos\beta| \quad (4)$$

Deep water conditions are assumed, giving the following relationship for incident wavenumber:

$$k_I = \frac{\omega_I^2}{g} \quad (5)$$

Similarly, the wavenumber for radiated waves is given by:

$$k_e = \frac{\omega_e^2}{g} \quad (6)$$

The pressure at a point in the fluid is given by Bernoulli's equation for unsteady flow:

$$p = -\rho\left(\frac{\partial\Phi}{\partial t} + \frac{1}{2}|\nabla\Phi|^2 + g\,z\right) \quad (7)$$

where ρ is water density. Neglecting second and higher order terms, the oscillatory pressure acting on the ship hull is given by:

$$p = -\rho\left(i\,\omega_e - U\,\frac{\partial}{\partial x}\right)\left[\phi_I + \phi_D + \sum_{j=1}^{6}\eta_j\phi_j\right] - \rho g\zeta_3 \quad (8)$$

The last term of the above equation denotes the oscillatory pressure due to hydrostatic pressure, with ζ_3 being the oscillatory vertical displacement given by:

$$\zeta_3 = \eta_3 + y\eta_4 - x\eta_5 \quad (9)$$

The oscillatory motions of the ship can be solved as follows:

$$\left\{-\omega_e^2\left([M]+[A]\right) + i\omega_e[B] + [C]\right\}\{\eta\} = \left\{F^I + F^D\right\} \quad (10)$$

where $[M]$ is the ship mass matrix, $[A]$ is the added mass matrix, $[B]$ is the radiation damping matrix, $[C]$ is the hydrostatic stiffness matrix, $\left\{F^I\right\}$ is the incident wave force vector, and $\left\{F^D\right\}$ is the wave diffraction force vector. The added mass and damping matrix terms are given by:

$$A_{jk} = -\frac{\rho}{\omega_e}\int_{S_b}\left[\text{Imag}(\phi_k) - \frac{U}{\omega_e}\,\text{Real}\left(\frac{\partial\phi_k}{\partial x}\right)\right] n_j\,dS \quad (11)$$

$$B_{jk} = -\rho\int_{S_b}\left[\text{Real}(\phi_k) - \frac{U}{\omega_e}\,\text{Imag}\left(\frac{\partial\phi_k}{\partial x}\right)\right] n_j\,dS \quad (12)$$

where S_b denotes the mean wetted surface of the ship. The normals for each motion mode k are given by:

$$n_1 = n_x \quad (13)$$
$$n_2 = n_y \quad (14)$$
$$n_3 = n_z \quad (15)$$
$$n_4 = yn_z - zn_y \quad (16)$$
$$n_5 = zn_x - xn_z \quad (17)$$
$$n_6 = xn_y - yn_x \quad (18)$$

where n_x, n_y, and n_z are the directional cosines for the unit normal pointing outward from the hull. The hydrostatic stiffness matrix $[C]$ includes the influence of the oscillatory vertical displacement given by Equation (9). The wave excitation forces on the ship are given by:

$$F_j^I = \rho\,\omega_e\int_{S_b}\left(i\phi_I - \frac{U}{\omega_e}\,\frac{\partial\phi_I}{\partial x}\right) n_j\,dS \quad (19)$$

$$F_j^D = \rho\,\omega_e\int_{S_b}\left(i\phi_D - \frac{U}{\omega_e}\,\frac{\partial\phi_D}{\partial x}\right) n_j\,dS \quad (20)$$

The incident wave potential is given by:

$$\phi_I = \frac{i\,g\,a}{\omega_I}\,\exp\left[-i\,k_I\,(x\cos\beta - y\sin\beta)\right] \times \exp(k_I\,z_{wl}) \quad (21)$$

where g is gravitational acceleration, a is incident wave amplitude, and z_{wl} is elevation relative to the calm water surface. The incident wave potential of Equation (21) is formulated such that the wave crest is located is aligned with x and y for the ship centre of gravity at time $t = 0$.

THEORY FOR SOLUTION OF RADIATION AND DIFFRACTION FORCES IN FREQUENCY DOMAIN

A source distribution method is used to solve for the radiation and diffraction potentials presented in the previous section. The radiated or diffracted velocity potential at a location in the fluid domain is expressed as follows:

$$\phi(\vec{x}) = \frac{1}{4\pi}\int_{S_b} G(\vec{x},\vec{x}_s,U,\omega_e)\,\sigma(\vec{x}_s)\,dS \quad (22)$$

where $\vec{x}_s$ is source location on the surface of the ship, $G(\vec{x},\vec{x}_s)$ is the Green function describing the flow at $\vec{x}$ caused by a source of unit strength at $\vec{x}_s$, and $\sigma(\vec{x}_s)$ is the strength of the source at $\vec{x}_s$. The Green function ideally satisfies the continuity condition and all boundary conditions, with the exception of the following normal velocity boundary condition on the hull surface:

$$\frac{\partial\phi(\vec{x})}{\partial n} = v_n(\vec{x}) \text{ on } S_b \quad (23)$$

where $v_n(\vec{x})$ is the flow normal velocity on the hull surface. The source strengths are solved such that the following equation is satisfied:

$$\frac{1}{4\pi}\int_{S_b}\frac{\partial G(\vec{x},\vec{x}_s,U,\omega_e)}{\partial n_{\vec{x}}}\,\sigma(\vec{x}_s)\,dS = v_n(\vec{x}) \text{ on } S_b \quad (24)$$

For radiation potentials, the hull boundary condition is:

$$\frac{\partial\phi_k(\vec{x})}{\partial n} = i\,\omega_e\,n_k \text{ on } S_b \quad (25)$$

For the wave diffraction potentials, the hull boundary condition is:

$$\frac{\partial \phi_D(\vec{x})}{\partial n} = -\frac{\partial \phi_I(\vec{x})}{\partial n} \text{ on } S_b \quad (26)$$

For solutions using a panelled hull, the radiation and source strengths are solved by satisfying the following discretized form of Equation (24):

$$[\partial D(\omega_e)/\partial n]\ \{\sigma\} = \{\partial \phi/\partial n\} \quad (27)$$

$[D(\omega_e)]$ is the velocity potential influence matrix. Equation (27) is solved for all 6 radiation modes and also for wave diffraction. After the source strengths $\{\sigma\}$ have been solved, velocity potentials are determined as follows:

$$\{\phi\} = [D(\omega_e)]\ \{\sigma\} \quad (28)$$

Simplified Treatment of Forward Speed Effects on Radiation Coefficients

The present method assumes low forward speed, allowing radiation potentials at forward speed to be evaluated using radiation potentials computed at zero speed. When evaluating velocity potentials, the frequency domain Green function for zero forward speed is used (Telste and Noblesse 1986). The dependence of encounter frequency on ship speed is fully considered; however, utilization of the zero speed Green function means that the influence of ship speed on the free surface boundary condition is not fully modelled.

When considering the radiation boundary condition on the ship at forward speed, the steady flow due to ship forward speed is approximated by uniform flow, neglecting the influence of the steady scattered flow. Although more sophisticated potential flow models are often used for modelling the steady flow due to ship forward speed (Chen and Malenica 1998), they often don't significantly improve accuracy, likely because of the importance of viscous effects for steady flow.

The current simplified treatment enables forward speed radiation potentials to be evaluated as follows:

$$\phi_1(U,\omega_e) = \phi_1(0,\omega_e) \quad (29)$$
$$\phi_2(U,\omega_e) = \phi_2(0,\omega_e) \quad (30)$$
$$\phi_3(U,\omega_e) = \phi_3(0,\omega_e) \quad (31)$$
$$\phi_4(U,\omega_e) = \phi_4(0,\omega_e) \quad (32)$$
$$\phi_5(U,\omega_e) = \phi_5(0,\omega_e) + \frac{U}{i\omega_e}\,\phi_3(0,\omega_e) \quad (33)$$
$$\phi_6(U,\omega_e) = \phi_6(0,\omega_e) - \frac{U}{i\omega_e}\,\phi_2(0,\omega_e) \quad (34)$$

The added masses and damping coefficients of Equations (11) and (12) can then be expressed using speed-independent terms as follows:

$$A_{jk}(U,\omega_e) = A^0_{jk}(\omega_e) + UA^U_{jk}(\omega_e) + U^2A^{UU}_{jk}(\omega_e) \quad (35)$$
$$B_{jk}(U,\omega_e) = B^0_{jk}(\omega_e) + UB^U_{jk}(\omega_e) + U^2B^{UU}_{jk}(\omega_e) \quad (36)$$

The speed-independent terms in the above equations are evaluated using the zero-speed radiation potentials $\phi_k(0,\omega_e)$ and their x-derivatives $\partial\phi_k(0,\omega_e)/\partial x$.

Radiation Terms at Zero and Infinite Frequency Limits

Radiation terms at very low and very high frequencies can be approximated using using zero and infinite frequency limits. In the vicinity of these limits, the radiation potentials can be expressed using normalized radiation potentials as follows:

$$\phi_k(\omega_e) \approx i\,\omega_e\,\phi'_k(\omega_e=0) \text{ for } \omega_e \to 0 \quad (37)$$
$$\phi_k(\omega_e) \approx i\,\omega_e\,\phi'_k(\omega_e=\infty) \text{ for } \omega_e \to \infty \quad (38)$$

In the present work using the Green function for zero forward speed, the associated limits at zero and infinite frequencies are:

$$G(\vec{x},\vec{x}_s,U,\omega_e=0) = \frac{1}{R(\vec{x},\vec{x}_s)} + \frac{1}{R_1(\vec{x},\vec{x}_s)} \quad (39)$$
$$G(\vec{x},\vec{x}_s,U,\omega_e=\infty) = \frac{1}{R(\vec{x},\vec{x}_s)} - \frac{1}{R_1(\vec{x},\vec{x}_s)} \quad (40)$$

where $R(\vec{x},\vec{x}_s)$ is the distance from the field point $\vec{x}$ to the source point $\vec{x}_s$, and $R_1(\vec{x},\vec{x}_s)$ is the distance from the field point $\vec{x}$ to the image of the source point $\vec{x}_s$. Note that the image of the source point $\vec{x}_s$ has coordinates $x_s, y_s, -z_{wl-s}$. Because the Green functions at the zero and infinite frequency limits are real, the normalized velocity potentials $\phi'_k(\omega_e=0)$ and $\phi'_k(\omega_e=\infty)$ are also real.

Experience with naval vessels indicates that the zero frequency approximation can be used when $\omega_e < 0.2\sqrt{g/L}$. Similarly, the infinite frequency approximation can be used when $\omega_e > 20\sqrt{g/L}$.

Suppression of Irregular Frequency Effects

When solving for source strengths and velocity potentials using Equations (22) and (24) and a Green function that satisfies the free surface boundary condition, encounter frequencies exist at which the solved flow potentials are mathematical correct but physically incorrect. These encounter frequencies are called "irregular" frequencies and are documented in the literature (Inglis and Price 1981; Lee and

Sclavounos 1989; Malenica and Chen 1998). A mathematical solution including irregular frequency effects has induced sloshing of water within the interior of the ship hull.

Irregular frequencies occur for surface-piercing hulls, and are typically confined to narrow ranges of higher encounter frequencies. For a ship with lateral symmetry, one set of irregular frequencies will exist for longitudinal modes (surge, heave, and pitch) and a second set of irregular frequencies will exist for lateral modes (sway, roll, and yaw). For numerical solutions, the width of each range of irregular frequencies will depend on the panelled mesh, with a finer mesh giving narrower ranges of irregular frequencies.

There are 3 commonly used approaches for dealing with irregular frequencies:

- Remove irregular frequencies from computations through visual inspection of computed added mass and damping coefficients to determine if any irregular frequencies are present;
- Suppress sloshing within the interior of the ship hull by placing a lid of panels within the hull at the free surface, applying a boundary condition of $\partial\phi/\partial z = 0$ on lid panels (Malenica and Chen 1998);
- Rather than using source distribution method, use direct method for solving velocity potentials, including approach of Lee and Sclavounos (1989) for eliminating irregular frequencies.

Visual inspection for irregular frequencies works generally well. Visual inspection can be assisted by examination of condition numbers for matrices used to solve source strengths (Equation (24)). An irregular frequency usually has a high condition number associated with it.

Application of lid panels for suppressing irregular frequencies is now widely used. Figure 6 gives an example of a generic frigate with a panelled lid at the free surface for suppressing irregular frequencies. The method is robust and is reasonably tolerant of geometric imperfections, such as the lid panels not covering the entire free surface inside the ship. For the generic frigate shown in Figure 6, the panelled lid covers 97 percent of the wetted length of the hull and 95 percent of the local wetted width. The lid method has a computational expense associated with solving for additional source strengths.

Direct methods appear to be less widely used than source distribution methods for solving radiation and diffraction potentials. Similarly, the direct method of Lee and Sclavounos (1989) for suppressing irregular frequencies appears to be less commonly used that the source distribution with lid method of Malenica and Chen (1998).

Figure 7 gives heave added mass and damping coefficients for a generical naval frigate, showing results from computations with and without the lid method for suppressing irregular frequencies. Figure 8 shows associated condition numbers for the influence matrix $[\partial D(\omega_e)\partial n]$. When no lid is present, irregular frequencies are associated with high local condition numbers for the influence matrix $[\partial D(\omega_e)\partial n]$ in Equation (27). When a lid is used to suppress irregular frequencies, the numerical solution is sufficiently robust regardless of high condition numbers at certain frequencies.

NUMERICAL EVALUATION OF RADIATION AND DIFFRACTION FORCES IN THE FREQUENCY DOMAIN

The theory described above has been implemented as part of the ShipMo3D ship motion library for computing ship motions in waves in the frequency and time domains.

Programming Language

When selecting a programming language, several factors were considered, including the following:

- Suitability for numerical programming, including support for complex numbers and availability of numerical libraries;
- Support for contemporary programming practices, including object-oriented programming;
- Ease of programming, including automatic memory management;
- Numerical performance.

The majority of the software has been developed using the C# programming language (Griffiths 2012). C# has very good support for numerical programming, with excellent libraries available. C# is similar to other modern programming languages, especially Java; thus, it ease relatively easy to find programmers who are proficient with C# or who can be trained with minimal effort. Like Java, C# includes automatic memory management.

Complied C# software currently runs in the .NET virtual machine. In general, software compiled for a virtual machine runs more slowly than software that has been compiled for native hardware. Fortunately, C# can easily access software libraries that run on native hardware. For the ShipMo3D software library, some numerically intensive components have been written in C++ and compiled natively to enable maximum performance. Based on software profiling, it is estimated that the usage of C# for the present

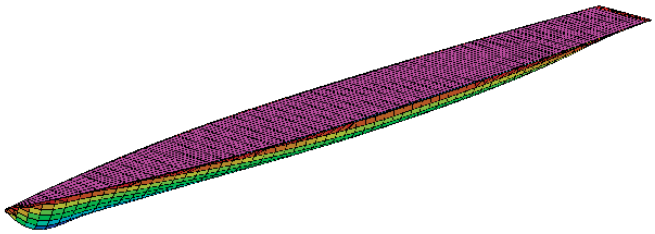

Figure 6: Wet Panelled Hull and Panelled Lid for Generic Naval Frigate (Lid Panels Shown in Magenta)

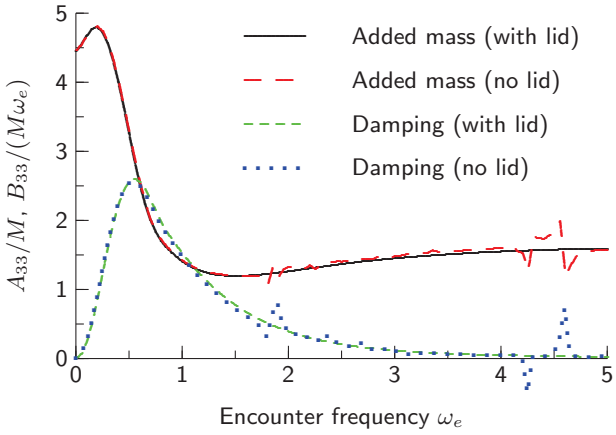

Figure 7: Heave Added Mass and Damping Coefficients for Generic Naval Frigate

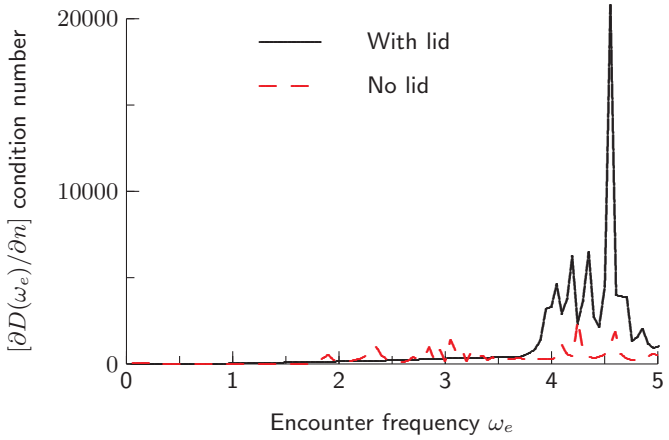

Figure 8: Longitudinal Mode Condition Numbers for Generic Naval Frigate

software has a performance of penalty of less than 10 percent relative to C++ natively compiled software. Microsoft recently released a native compiler for C#, which will give further performance improvement.

Solution of Radiation Potentials

The radiation potential source strength vectors $\{\sigma_k\}$ and radiation potential vectors $\{\phi_k\}$ are solved for modes $k = 1-6$ using Equation (27) followed by Equation (28). When formulating the influence matrix terms, the zero speed Green function is considered as follows:

$$G(\vec{x},\vec{x}_s,\omega_e) = \frac{1}{R(\vec{x},\vec{x}_s)} - \frac{1}{R_1(\vec{x},\vec{x}_s)} + \widetilde{G}_\infty(\vec{x},\vec{x}_s,\omega_e) \quad (41)$$

where R is the distance between the field point and the source point, R_1 is the distance between the field point and the image of the source point, and $\widetilde{G}_\infty(\vec{x},\vec{x}_s,\omega_e)$ is the frequency dependent portion of the Green function relative to its value at infinite frequency. The influence matrix terms are then evaluated as:

$$D_{ij}(\omega_e) = \frac{1}{4\,\pi}\left(\int_{S_j}\frac{1}{R(\vec{x}_i,\vec{x}_s)}\,d\vec{x}_s - \int_{S_j}\frac{1}{R_1(\vec{x}_i,\vec{x}_s)}\,d\vec{x}_s + A_j\sum_{m=1}^{N_{Gauss}} w_m\,\widetilde{G}_\infty(\vec{x},\vec{x}_{s-jm},\omega_e)\right) \quad (42)$$

where S_j is the surface of source j, $\vec{x}_i$ is the centroid of panel i, A_j is the area of source panel j, N_{Gauss} is the number of points on the source panel used for Gauss quadrature, w_m is the Gauss quadrature weight for quadrature index m, and $\vec{x}_{s-mj}$ is the point on the source panel j with quadrature index m. The $1/R$ and $1/R_1$ integrals in Equation (42) can be evaluated with high accuracy using methods described by Garrison (1978). Second-order Gauss quadrature (4 points per source panel) is typically used. Note that the integration of the Green function in Equation (42) has been formulated such that it is most accurate at high frequencies, where solutions can be sensitive to errors introduced by using Gauss quadrature for the frequency dependent portion.

The method has been implemented using the assumption of lateral symmetry for ship geometries. Consequently, velocity potentials and source strengths for longitudinal modes (surge, heave, and pitch) are even functions of the lateral coordinate y. Similarly, velocity potentials and source strengths for lateral modes (sway, roll, and yaw) are odd functions of lateral coordinate y. The assumption of lateral symmetry gives significant reductions in computational

times for evaluation of influence matrices and solution of source strengths.

As mentioned previously, a lid of source panels is commonly used to suppress irregular frequencies. The velocity potentials on the ship hull are then evaluated as follows:

$$\left\{\phi_k^{hull}\right\} = \left[\begin{array}{c|c} D^{hull-hull}(\omega_e) & D^{hull-lid}(\omega_e) \end{array}\right] \left\{\begin{array}{c} \sigma_k^{hull} \\ \hline \sigma_k^{lid} \end{array}\right\} \quad (43)$$

where $\left\{\phi_k^{hull}\right\}$ is the vector of velocity potentials on the hull for mode k, $\left[D(\omega_e)^{hull-hull}\right]$ is the velocity potential influence matrix for the hull, $\left[D(\omega_e)^{hull-lid}\right]$ is the velocity potential influence matrix of the lid on the hull, $\left\{\sigma_k^{hull}\right\}$ is the vector of hull source strengths for mode k, and $\left\{\sigma_k^{lid}\right\}$ is the vector of lid source strengths for mode k. The source strengths including both the hull and lid are solved by satisfying the following:

$$\left[\begin{array}{c|c} \partial D^{hull-hull}(\omega_e)/\partial n & \partial D^{hull-lid}(\omega_e)/\partial n \\ \hline \partial D^{lid-hull}(\omega_e)/\partial n & \partial D^{lid-lid}(\omega_e)/\partial n \end{array}\right] \times \left\{\begin{array}{c} \sigma_k^{hull} \\ \hline \sigma_k^{lid} \end{array}\right\} = \left\{\begin{array}{c} \partial\phi_k/\partial n \\ \hline 0 \end{array}\right\} \quad (44)$$

When evaluating the frequency dependent portion of the Green function, $\tilde{G}_\infty(\vec{x}, \vec{x}_s, \omega_e)$, there can be a problem when evaluating the influence of a lid panel on itself because the function is singular when the field point is the same as the source point and it lies on the water plane. This problem can be circumvented by using Gauss quadrature of even order (e.g., 2 or 4) when evaluating Equation (42) and associated derivatives.

Solution of Diffraction Potentials

The wave diffraction potentials are solved in a manner similar to that used for solving the radiation potentials. To take advantage of the lateral symmetry of the ship, the incident wave potential of Equation (21) is divided into components that are even and odd functions of the lateral coordinate y. The even and odd diffraction potentials are solved separately and then combined to yield the total diffraction potentials on the ship hull. A lid method is applied to suppress irregular frequency effects.

When solving diffraction potentials, a large amount of computation effort can be expended evaluating Green functions and performing the lower upper (LU) factorization for solution of the diffraction equivalents for Equations (44) and (43). For the example generic frigate, radiation computations for 100 encounter frequencies ω_e (0.05, 0.10, ..., 5.0 rad/s) provide excellent resolution of added mass and damping coefficients. In contrast, a large number of diffraction computations must be performed to capture the range of conditions likely to be encountered by a ship. For the example generic frigate, 12506 sets of diffraction computations must be performed to capture 26 ship speeds U (-10, -8, ..., 40 knots), 13 relative sea directions β (0, 15, ..., 180 degrees), and 37 incident incident wave frequencies ω_I (0.20, 0.25, ..., 2.0 rad/s). Fortunately, great savings in computational times and acceptable accuracy can be achieved by utilizing influence matrices $[D(\omega_e)]$ and $[\partial D(\omega_e)/\partial n]$ at encounter frequencies that are near but necessarily equal to the encounter frequency for the actual seaway. The diffraction source strength potential vector for a given seaway is based on the following:

$$\begin{aligned}\{\sigma_D(U,\beta,\omega_I)\} = {} & w_{lower}\ \left\{\sigma_D(U,\beta,\omega_I,[\partial D(\omega_e^{lower})]/\partial n)\right\} \\ & + w_{upper}\ \left\{\sigma_D(U,\beta,\omega_I,[\partial D(\omega_e^{upper})]/\partial n)\right\} \end{aligned} \quad (45)$$

where the diffraction source strength vector is solved twice, once using the influence matrices for encounter frequency ω_e^{lower} and a second time using the influence matrices for encounter frequency ω_e^{upper}. The encounter frequencies satisfy the following:

$$\omega_e^{lower} \ \le\ \omega_e(U,\beta,\omega_I) \ \le\ \omega_e^{upper} \quad (46)$$

The weights w_{lower} and w_{upper} in Equation (45) are based on linear interpolation. After the diffraction source strengths have been evaluated for a given wave condition, the diffraction velocity potentials and their derivatives are evaluated using interpolated influence matrices. The solution times using the influence matrices for encounter frequencies ω_e^{lower} and ω_e^{upper} are fast because the influence matrices and the associated LU factorizations for $[\partial D(\omega_e^{lower})/\partial n]$ and $[\partial D(\omega_e^{upper})/\partial n]$ have already been computed for solving radiation coefficients. To save computational memory, the influence matrices and LU factorizations are only stored for two encounter frequencies at a time, and all wave conditions are scanned to determine which wave conditions satisfy Equation (46).

Figures 9 and 10 show predicted heave and pitch motions for the generic frigate travelling at 10 knots in head seas, with wave diffraction potentials computed directly and using the approximation of Equation (45). The excellent agreement between the two approaches indicates that the approximation of Equation (45) is acceptable.

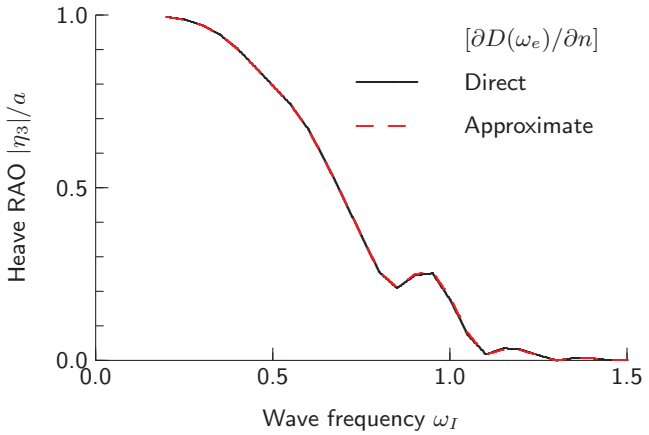

Figure 9: Heave Motions for Generic Naval Frigate Computed Directly and with Diffracted Wave Influence Matrix Approximation, 10 knots in Head Seas

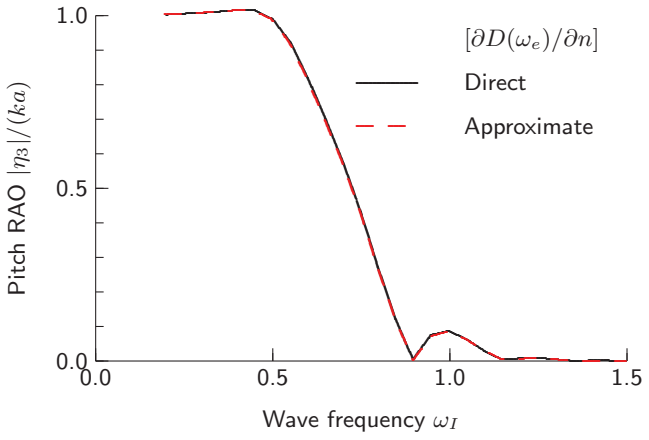

Figure 10: Pitch Motions for Generic Naval Frigate Computed Directly and with Diffracted Wave Influence Matrix Approximation, 10 knots in Head Seas

Parallel Processing

Parallel computing is now widely available on desktop computers. The implemented software exploits parallel computing in two ways. Evaluation of the influence matrix $[D(\omega_e)]$ and its derivatives is done using parallel `for` loops in C# (Griffiths 2012). Implementation of parallel processing is very easy because the elements of the influence matrices are independent of each other. During linear algebra operations, including solving systems of equations, the parallel computation capabilities of the Intel Math Kernel Library (Wang, Zhang, Shen, Zhang, Lu, Wu, and Wang 2014) are exploited by the Math.NET Numerics library (Math.NET Numerics 2015). Effort for implementing both of the above parallel capabilities was minimal.

Computational Times for Solution of Radiation Forces and Diffraction Forces

Table 1 gives computational times on a desktop workstation with 16 processor cores for radiation and diffraction forces for the generic frigate. Radiation forces are evaluated for 100 encounter frequencies ω_e (0.00, 0.05, ..., 5.00 rad/s). Diffraction forces are evaluated for 12506 wave conditions, which capture 26 ship speeds U (-10, -8, ..., 40 knots), 13 relative sea directions β (0, 15, ..., 180 degrees), and 37 incident incident wave frequencies ω_I (0.20, 0.25, ..., 2.0 rad/s). The diffraction force solution time per wave condition is approximately half of the radiation force solution time per encounter frequency because the diffraction force solution uses influence matrixes and LU factorizations from the radiation force solutions. Further speed gains are likely achievable through implementation of native C++ code and parallel computation at critical areas that could be identified through run-time profiling.

Radiation forces for 100 encounter frequencies	1168 s
Radiation forces average time per frequency	1.2 s
Diffraction forces for 12506 wave conditions	7953 s
Diffraction forces average time per wave condition	0.6 s

Table 1: Radiation and Diffraction Computation Times for Generic Frigate

THEORY FOR SOLUTION OF RADIATION AND DIFFRACTION FORCES IN THE TIME DOMAIN

Wehausen (1971) and Mei (1983) discuss hydrodynamic forces in the time domain, including evaluation of time domain coefficients from frequency domain coefficients. The

motion of a floating body in waves may be evaluated in the time domain as follows:

$$\begin{aligned}([M] + [A(U,\infty)])\ \{\ddot{\eta}(t)\}\ +\ [b(U)]\ \left\{\dot{\eta(t)}\right\} \\ +\ \int_0^\infty [K(U,\tau)]\,\{\dot{\eta}(t\ -\ \tau)\}\ d\tau \\ +\ ([C]\ +\ [c(U)])\ \{\eta(t)\} \\ =\ \left\{F^I(t)\ +\ F^D(t)\right\} \end{aligned} \quad (47)$$

where $[b(U)]$ is the speed dependent damping matrix in the time domain, $[K(U,\tau)]$ is the retardation function matrix for delay time τ, and $[c(U)]$ is the speed dependent stiffness matrix in the time domain.

The retardation functions $K_{jk}(U,\tau)$ can be determined from frequency domain added mass or damping coefficients as follows:

$$\begin{aligned} K_{jk}(\tau) &= -\frac{2}{\pi}\int_0^\infty [A_{jk}(U,\omega_e)\ -\ A_{jk}(U,\infty)] \\ &\qquad \times \omega_e\ \sin\omega_e\tau\ d\omega_e \end{aligned} \quad (48)$$

$$K_{jk}(\tau) = \frac{2}{\pi}\int_0^\infty B_{jk}(U,\omega_e)\ \cos\omega_e\tau\ d\omega_e \quad (49)$$

When selecting between the above two equations for evaluating retardation functions, Equation (49) is primarily used in the present method because damping coefficients tend to approach their infinite frequency limits more quickly than do added masses. In a manner similar to that used for added mass and damping coefficients in the frequency domain, the speed-dependent retardation functions are evaluated using speed-independent terms as follows:

$$K_{jk}(U,\tau) = K^0_{jk}(\tau)\ +\ U\ K^U_{jk}(\tau)\ +\ U^2\ K^{UU}_{jk}(\tau) \quad (50)$$

The hydrodynamic damping and stiffness terms are as follows when the steady flow is modelled as the uniform steady flow:

$$b_{jk}(U) = U\ \rho\int_{S_b}\frac{\partial\phi'_k(0,\infty)}{\partial x}\ n_j\ dS \quad \text{for } k = 1-4 \quad (51)$$

$$\begin{aligned} b_{j5}(U) &= U\ \rho\int_{S_b}\frac{\partial\phi'_5(0,\infty)}{\partial x}\ n_j\ dS \\ &\quad +\ U\ A_{j3}(0,\infty) \end{aligned} \quad (52)$$

$$\begin{aligned} b_{j6}(U) &= U\ \rho\int_{S_b}\frac{\partial\phi'_6(0,\infty)}{\partial x}\ n_j\ dS \\ &\quad -\ U\ A_{j2}(0,\infty) \end{aligned} \quad (53)$$

$$c_{j5}(U) = U^2\ \rho\int_{S_b}\frac{\partial\phi'_3(0,0)}{\partial x}\ n_j\ dS \quad (54)$$

$$c_{j6}(U) = -\ U^2\ \rho\int_{S_b}\frac{\partial\phi'_2(0,0)}{\partial x}\ n_j\ dS \quad (55)$$

The incident wave elevation in the time domain can include a phase lead ϵ_I for the wave crest, and is formulated as:

$$\begin{aligned}\zeta_I(x,y,t)\ &= \\ &a\ \cos\left[\omega_e\,t\ +\ \epsilon_I\ -\ k_I\,(x\cos\beta\ -\ y\sin\beta)\right]\end{aligned} \quad (56)$$

Wave excitation forces in the time domain can be expressed in terms of frequency domain values as follows:

$$\begin{aligned} F^I_j(t) &= \left|F^I(U,\beta,\omega_I)\right| \\ &\quad \times\ \cos\left[\omega_e t\ +\epsilon_I\ +\ \epsilon_j\left(F^I(U,\beta,\omega_I)\right)\right] \end{aligned} \quad (57)$$

$$\begin{aligned} F^D_j(t) &= \left|F^D(U,\beta,\omega_I)\right| \\ &\quad \times\ \cos\left[\omega_e t\ +\epsilon_I\ +\ \epsilon_j\left(F^D(U,\beta,\omega_I)\right)\right] \end{aligned} \quad (58)$$

The phases ϵ_j of the incident and diffracted excitation forces for incident waves with zero phase angles are given by:

$$\epsilon_j\left(F^I_j(U,\beta,\omega_I)\right) = \arctan\frac{\text{Imag}\left\{F^I_j(U,\beta,\omega_I)\right\}}{\text{Real}\left\{F^I_j(U,\beta,\omega_I)\right\}} \quad (59)$$

$$\epsilon_j\left(F^D_j(U,\beta,\omega_I)\right) = \arctan\frac{\text{Imag}\left\{F^D_j(U,\beta,\omega_I)\right\}}{\text{Real}\left\{F^D_j(U,\beta,\omega_I)\right\}} \quad (60)$$

NUMERICAL EVALUATION OF RADIATION AND DIFFRACTION FORCES IN THE TIME DOMAIN

The C# library for computing forces and motions in the frequency domain also performs computations in the time domain.

Coordinate Systems

Motions in the time domain are ultimately given using the earth-fixed axis system shown in Figure 11. At each time step, a translating earth axis system, as shown in Figure 5, is used with properties based on the instantaneous location, speed, and heading of the ship. The seaway, which is defined in earth-fixed axes, is transformed to translating earth axes at each time step such that Equations (57) and (58) can be applied.

Evaluation of Retardation Functions

Before commencing a time domain simulation, the retardation function terms $K^0_{jk}(\tau)$, $K^U_{jk}(\tau)$, and $K^{UU}_{jk}(\tau)$ are evaluated for the ship based on the time step to be used for ship motion computations. Although Equation (47) indicates that the delay time τ goes to infinity when evaluating retardation forces, the retardation functions decay to zero

reasonably quickly, allowing a practical maximum to be applied to τ. A practical maximum τ_{max} of approximately $5\sqrt{L/g}$ is recommended.

Retardation function terms are evaluated using Equation (49). A practical maximum encounter frequency ω^* must be selected when evaluating retardation function terms, with a value of approximately $20\sqrt{g/L}$ recommended. When evaluating retardation functions, it has been found that the following approximation is very useful for modelling damping at high frequencies:

$$B_{ij}(\omega_e) \;=\; B_{ij}(\omega_e^*)\,\exp\left[\frac{-2\omega_e}{\omega_e^*}\,+\,2\right]\;\text{for}\;\omega_e > \omega_e^* \quad (61)$$

Equation (49) can then be evaluated as:

$$K_{jk}(\tau) \;=\; \frac{2}{\pi}\int_0^{\omega_e^*} B_{jk}(U,\omega_e)\,\cos\omega_e\tau\,d\omega_e + \frac{2}{\pi}\,B_{jk}(U,\omega_e^*)\left[\frac{\frac{2\,\cos(\omega_e^*\tau)}{\omega_e^*}\,-\,\tau\,\sin(\omega_e^*\tau)}{\frac{4}{\omega_e^{*\,2}}\,+\,\tau^2}\right] \quad (62)$$

Figure 12 shows the computed heave retardation function for the generic frigate at zero speed. The retardation function behaves as expected, decaying to zero after approximately 15 s.

The retardation force integral in Equation (47) is evaluated using the trapezoidal rule with delay time interval $\Delta\tau$. In practice, $\Delta\tau$ is often set equal to the time step size Δt for integration of ship motions. For some simulations, the simulation time step Δt has to be set to a small value, while the retardation delay time interval $\Delta\tau$ can be set to an integer multiple of Δt to maintain acceptable computation times. Simulation of launch and recovery (McTaggart, Roy, Steinke, Nicoll and Perrault 2012) is an example where small simulation time step sizes should be used due to interactions with stiff mechanical systems, but larger retardation delay time intervals can be used.

Nonlinear Forces from Incident Waves and Buoyancy

It is very common for time domain simulations of ship motions to include nonlinear forces from incident waves and buoyancy. These forces can be evaluated based on the instantaneous wetted hull surface at a given time step. The present method includes this capability; however, experience to date suggests that the combination of nonlinear incident wave and buoyancy with linear radiation and diffraction forces does not necessarily given improved motion predictions over linear incident wave and buoyancy forces.

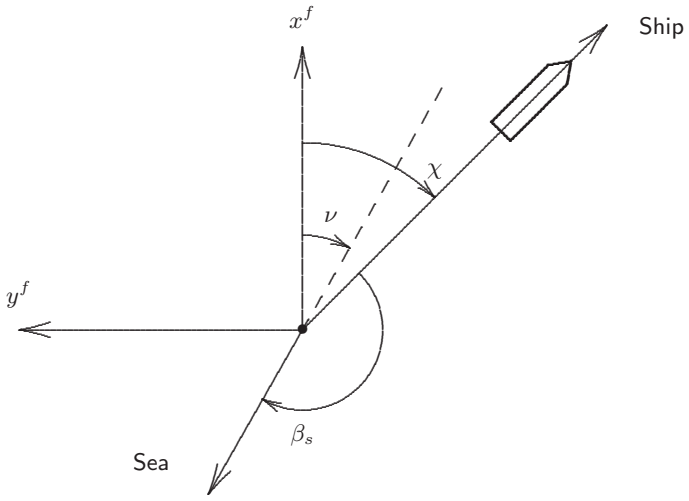

Figure 11: Earth-Fixed Axes for Computing Time Domain Motions

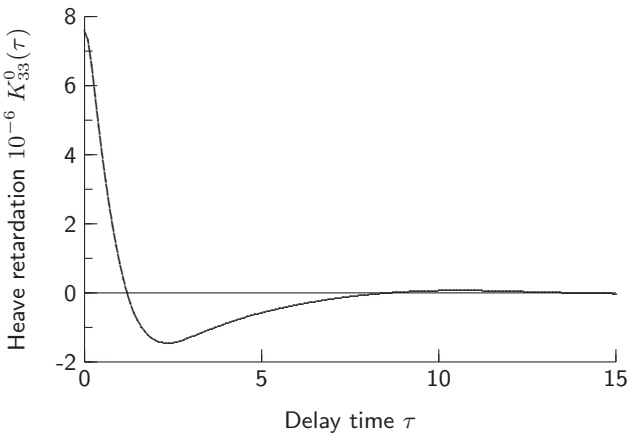

Figure 12: Heave Retardation Function at Zero Speed for Generic Frigate

Integration of Ship Motions

When selecting a numerical procedure for integration of ship motions, it should be noted that the evaluation of ship accelerations using Equation (47) can have significant computational cost. The present method evaluates the ship forces and associated accelerations only once per time step. Given the ship position $\{\eta\}$, velocity $\{\dot{\eta}\}$, and acceleration $\{\ddot{\eta}\}$ vectors at time t, the new position and velocity vectors at time $t + \Delta t$ are estimated as follows:

$$\{\widetilde{\eta}(t + \Delta t)\} = \{\eta(t)\} + \Delta t\,\{\dot{\eta}(t)\} + \frac{(\Delta t)^2}{2}\,\{\ddot{\eta}(t)\} \quad (63)$$

$$\{\widetilde{\dot{\eta}}(t + \Delta t)\} = \{\dot{\eta}(t)\} + \Delta t\,\{\ddot{\eta}(t)\} \quad (64)$$

The ship acceleration is then evaluated using the estimated ship position $\{\widetilde{\eta}\}$ and estimated ship velocity $\{\widetilde{\dot{\eta}}\}$:

$$\{\ddot{\eta}(t + \Delta t)\} = f\left(t + \Delta t,\, \widetilde{\eta}(t + \Delta t),\, \{\widetilde{\dot{\eta}}(t + \Delta t)\}\right) \quad (65)$$

The initial position and velocity estimates from Equations (63) and (64) are then replaced by the following:

$$\{\eta(t + \Delta t)\} = \{\eta(t)\} + \frac{\Delta t}{2}\,(\{\dot{\eta}(t)\} + \{\dot{\eta}(t + \Delta t)\}) \quad (66)$$

$$\{\dot{\eta}(t + \Delta t)\} = \{\dot{\eta}(t)\} + \frac{\Delta t}{2}\,(\{\ddot{\eta}(t)\} + \{\ddot{\eta}(t + \Delta t)\}) \quad (67)$$

The above set of equations has proven to provide very good stability for ship motion simulations.

Computation Times for Ship Motion Simulations

Table 2 gives ratios of computation times for the generic frigate in a random unidirectional seaway. The seaway is modelled using a Bretschneider spectrum with 33 discrete seaway components. A time step size of 0.2 s is used. The simulations run 1000 times faster than real time when using linear forces and incident waves and buoyancy, slowing to 16 times faster than real time when using nonlinear forces. Computational times are largely dependent on the number of wave components used to model a seaway; thus, times are very fast when simulating regular seaways and are slower when simulating random multidirectional seaways requiring many wave components.

Linear forces from incident waves and buoyancy	0.001
Nonlinear forces from incident waves and buoyancy	0.062

Table 2: Ratio of Computation Time to Simulated Time for Generic Frigate in Random Unidirectional Seaway

VALIDATION

The ship motion predictions have been validated extensively using data from model tests and sea trials (McTaggart 2010, McTaggart and Marly 2015). Much of the model test validation data is available in the public domain, including the steered warship model of Lloyd and Crossland (1990), the hydroelastic frigate model of McTaggart, Datta, Stirling, Gibson and Glen (1997), and the oceanographic research vessel model of Minnick, Hanyok, Tomaszek, Melendez, Turner, Park, Belenky, and Bassler (2012). Detailed data from a naval destroyer seakeeping trial (McTaggart and Stredulinsky 2004) was recently published on the internet with the title "HMCS Nipigon 1997 Seakeeping Trial Data".

Validation efforts have focussed on conditions where the software is expected to be routinely applied, with forward speed Froude numbers up to 0.4 and significant wave heights up to 7.5 m. Because the present paper addresses radiation and diffraction forces, presented validation results are limited to heave and pitch. For other modes, appendage forces and hull viscous forces are significant, and validation results have been presented elsewhere (McTaggart 2010, McTaggart 2014, McTaggart and Marly 2015).

Regular Seas Validation

Regular seas validation has been conducted using the steered warship model of Lloyd and Crossland (1990) and the hydroelastic frigate model of McTaggart, Datta, Stirling, Gibson and Glen (1997). Figures 13 and 14 shows heave and pitch motions of the steered warship model in stern quartering and bow quartering seas at a Froude number of approximately 0.27. The presented stern quartering seas conditions include high values of U/ω_e, challenging inherent assumptions with using the frequency domain Green function for zero forward speed. Fortunately, the numerical predictions give good agreement with the model tests in both stern quartering and bow quartering seas. The excellent agreement between predictions in the frequency and time domains verifies that the time domain implementation of forces from the frequency domain is correct.

Random Seas Validation

Validation of predictions in random seas has been performed using the naval destroyer sea trial of McTaggart and Stredulinsky (2004). In addition, McTaggart and Marly

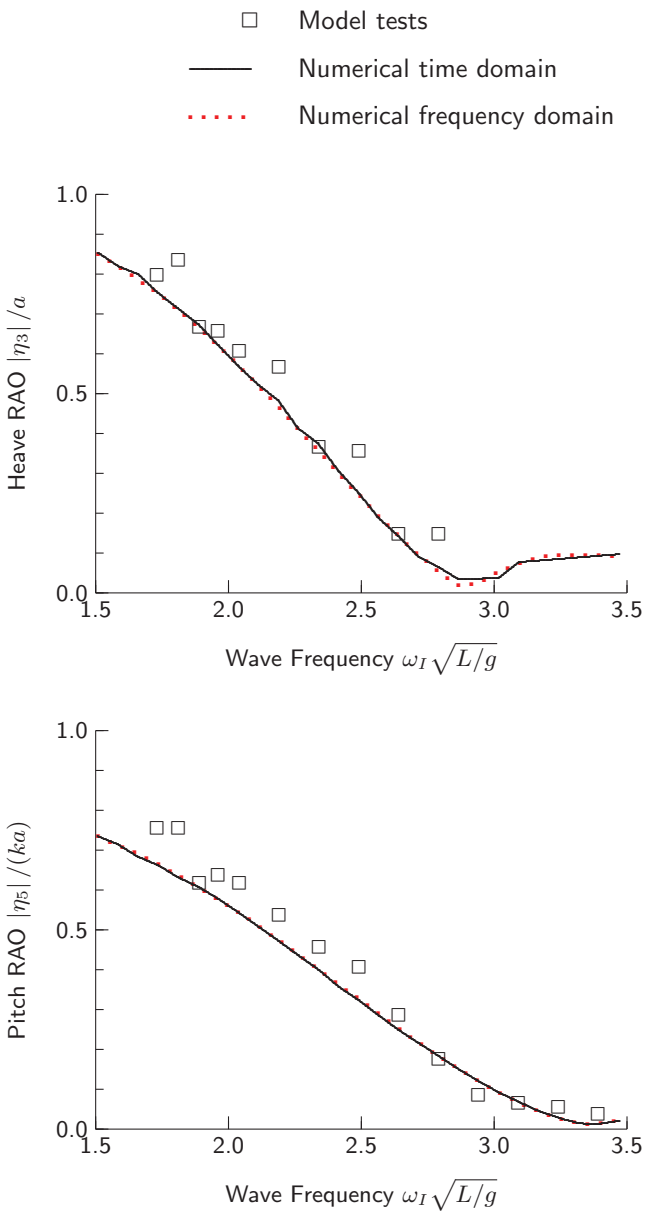

Figure 13: Steered Warship Heave and Pitch RAOs, Bow Quartering Seas at 30 degrees, Froude Number 0.27

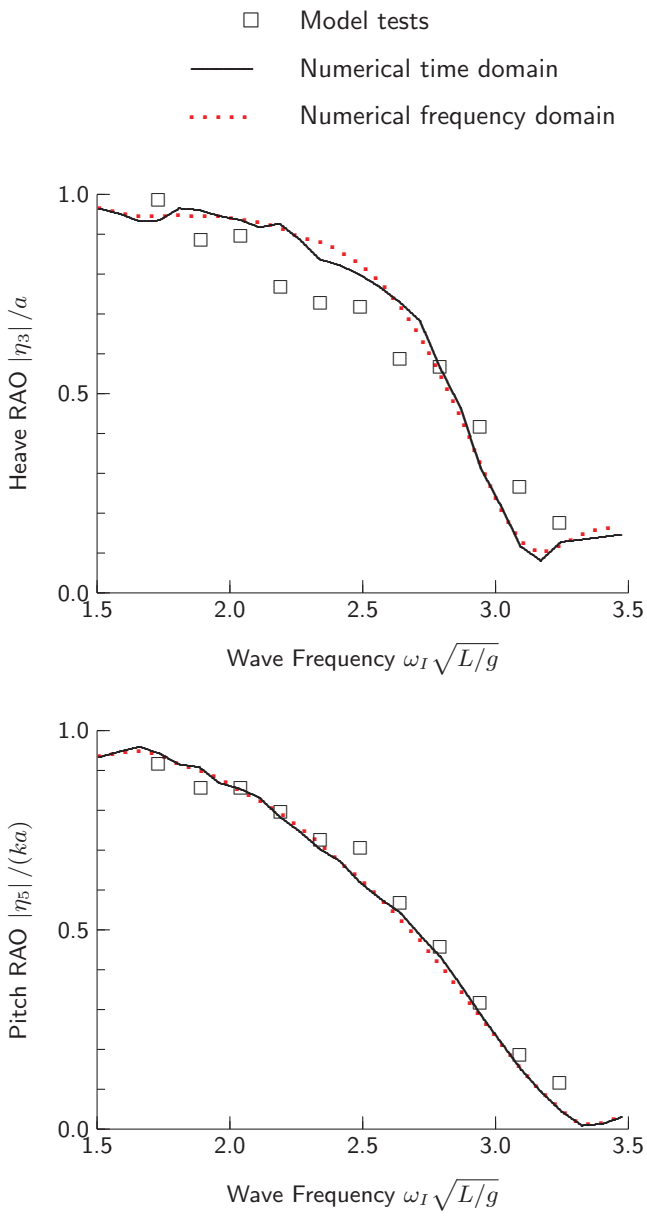

Figure 14: Steered Warship Heave and Pitch RAOs, Stern Quartering Seas at 150 degrees, Froude Number 0.26

(2015) present validation using the model tests of Minnick, Hanyok, Tomaszek, Melendez, Turner, Park, Belenky, and Bassler (2012) for an oceanographic research vessel.

When considering practical application of numerical seakeeping predictions, statistics regarding the ratio of predicted to measured values can provide useful insight. Table 3 gives ratios of predicted to experimentally derived motions in Sea State 6 for the steered warship model of Lloyd and Crossland (1990). The model tests were conducted in regular waves with steepness H/λ of 1/50. For the present random seas validation, a long-crested seaway is modelled using a Bretschneider spectrum with significant wave height of 5.0 m and peak wave period of 12.4 s. The experimental motions have been computed based on experimental RAOs and the model scaled to a full-scale length of 111.6 m. Table 3 gives statistics based on frequency domain predictions and experimentally derived values for 14 different combinations of ship speed and relative sea heading, with ship speeds ranging from 11.6 knots to 23.8 knots and headings ranging from stern quartering to bow quartering. The statistics indicate that predicted RMS motions are typically within 10 percent of values based on experiments, and prediction zero-crossing periods are typically within 5 percent of measured values.

Table 4 gives statistics for ratios of predicted to measured sea trial motions for HMCS Nipigon (McTaggart and Stredulinsky 2004). The statistics are based on 16 sea trial runs with ship speeds ranging from 8 to 16 knots, nominal relative sea directions of stern quartering, beam, and bow quartering, and significant wave heights ranging from 3.67 m to 5.82 m. The numerical predictions were performed in the frequency domain using the measured directional wave spectra from the sea trials. Table 4 indicates that the numerical predictions of RMS motion and zero-crossing period are typically within 15 percent of measured values. The accuracy of predictions for the HMCS Nipigon sea trial is less than the accuracy for the derived steered warship motions. Contributing factors to the lesser accuracy for HMCS Nipigon could include errors in measured directional sea spectra and nonlinearities caused by the moderately high seas.

	Mean	Deviation
RMS Heave	1.03	0.05
Heave T_z	1.00	0.02
RMS pitch	0.92	0.12
Pitch T_z	1.0	0.03

Table 3: Ratio of Predicted Motions to Motions Derived from Model Tests for Steered Warship in Sea State 6

	Mean	Deviation
RMS Heave	0.95	0.15
Heave T_z	0.99	0.09
RMS pitch	1.10	0.14
Pitch T_z	1.08	0.15

Table 4: Ratio of Predicted to Sea Trial Motions for Naval Destroyer HMCS Nipigon

CONCLUSIONS

Radiation and diffraction forces acting on ships with moderate forward speed are computed in the frequency domain using a three-dimensional method with Green function for zero forward speed. The method is efficient, robust, and acceptably accurate for ships in moderate wave conditions travelling with forward speed Froude numbers up to approximately 0.4. Using the Green function method eliminates the need for panelling the free surface associated with Rankine methods. Irregular frequencies associated with the Green function method for a surface piercing hull are eliminated by covering the waterplane area with lid panels and imposing a zero vertical velocity boundary condition.

Computation speed for diffraction computations is increased by using velocity potential influence matrices from radiation computations for a moderate number of wave encounter frequencies. This approximation reduces the time required for diffraction computations by approximately 50 percent, with sample computed ship motions showing no difference from motion predictions using directly computed influence matrices.

Radiation and diffraction force terms for time domain computations are evaluated using terms previously computed in the frequency domain. An approximation for radiation damping at high encounter frequencies is introduced for evaluation of time domain retardation functions.

Validation has been performed using model test and sea trials data available in the public domain. Validation results show very good agreement between predicted and observed values. Somewhat surprisingly, the good agreement is maintained even in stern quartering sea conditions for which U/ω_e is high, causing significant violation of assumptions regarding the free surface boundary condition when using the zero speed Green function. Excellent agreement

between predictions in the frequency and time domains indicates that the transformation of forces from the frequency domain to the time domain is correct.

REFERENCES

Chen, X.B. and S. Malenica. "Interaction Effects of Local Steady Flow on Wave Diffraction-Radiation at Low Forward Speed." *International Journal of Offshore and Polar Engineering*, Volume 8, Number 2, 1998.

Garrison, C.J. "Hydrodynamic Loading of Large Offshore Structures." *Numerical Methods in Offshore Engineering*, editors O.C.Zienkiewicz, R.W. Lewis and K.G. Stagg, Chichester, England: John Wiley & Sons, 1978.

Griffiths, I. *Programming C# 5.0*, O'Reilly & Associates, Sebastopol, California, 2012.

HMCS Nipigon 1997 Seakeeping Trial Data, http://open.canada.ca/data/en/dataset/2457d303-8449-4f4e-af79-811ea747e3f5, Accessed 24 April 2015.

Inglis, R.B. and W.G. Price. "Irregular Frequencies in Three Dimensional Source Distribution Techniques." *International Shipbuilding Progress*, Volume 28, Number 319, 1981.

Lee, C.-H., J.S. Letcher, R.G. Mack II, J.N.Newman, D.M. Shook and E. Stanley. "Integration of Geometry Definition and Wave Analysis Software." *21st International Conference on Offshore Mechanics and Arctic Engineering*, June, 2002.

Lee, C.-H. and P.D. Sclavounos. "Removing the Irregular Frequencies from Integral Equations in the Wave-Body Interactions." *Journal of Fluid Mechanics*, Volume 207, pp. 393-418, 1989.

Lloyd, A.R.J.M. and P. Crossland. "Motions of a Steered Model Warship in Oblique Waves." *Transactions, Royal Institution of Naval Architects*, Volume 132, 1990.

Malenica, S. and X.B. Chen. "On the Irregular Frequencies Appearing in Wave Diffraction-Radiation Solutions.", *International Journal of Offshore and Polar Engineering*, Volume 8, Number 2, 1998.

Math.NET Numerics, http://numerics.mathdotnet.com/, Accessed 23 April 2015.

McTaggart, K.A. *Three Dimensional Ship Hydrodynamic Coefficients Using the Zero Forward Speed Green Function*, DRDC Atlantic TM 2002-059, Defence Research and Development Canada – Atlantic, 2002.

McTaggart, K.A. "Verification and Validation of ShipMo3D Ship Motion Predictions in the Time and Frequency Domains." *International Towing Tank Conference Workshop on Seakeeping: Verification and Validation for Non-linear Seakeeping Analysis*, Seoul, Korea, 2010.

McTaggart, K.A. *Validation of ShipMo3D Version 3.0 User Applications for Simulation of Ship Motions* DRDC Atlantic TM 2011-306, Defence Research and Development Canada – Atlantic, 2014.

McTaggart, K., I. Datta, A. Stirling, S. Gibson and I. Glen. "Motions and Loads of a Hydroelastic Frigate Model in Severe Seas." *Transactions, Society of Naval Architects and Marine Engineers*, Volume 105, 1997.

McTaggart, K.A. and J.-F. Marly. "Seakeeping of a Research Vessel with Azimuthing Propellers." *34th International Conference on Ocean, Offshore and Arctic Engineering*, St. John's, Newfoundland, 2015.

McTaggart, K.A., A. Roy, D. Steinke, R. Nicoll and D. Perrault. "Simulation of Small Boat Launch and Recovery from a Ship with a Crane." *American Society of Naval Engineers Launch and Recovery Symposium*, Linthicum, Maryland, 2012.

McTaggart, K. and D. Stredulinsky. "Validation of Ship Motion Predictions with Sea Trials Data for a Naval Destroyer in Multidirectional Seas." *25th Symposium on Naval Hydrodynamics*, St. John's, Canada, 2004.

Mei, C.C. *The Applied Dynamics of Ocean Surface Waves*, John Wiley & Sons, New York, 1983.

Minnick, L.M., L.W. Hanyok, H.A. Tomaszek, M.P. Melendez, C.R. Turner, J.T. Park, V. Belenky, and C.C. Bassler. *Model-Scale Experiment of the Seakeeping Performance for R/V Melville, Model 5720*, Hydromechanics Department Report NSWCCD-50-TR-2012/035, Naval Surface Warfare Center Carderock Division, 2012.

Qiu W., H. Peng, S.M. Calisal and J. Wang, "Computation of Hydrodynamic Interaction of Multiple Bodies in Waves with a Panel-Free Method." *24th International Symposium on Offshore Mechanics and Arctic Engineering*, Halkidiki, Greece, 2005.

Papanikolaou, A.D. and T.E. Schellin. "A Three-Dimensional Panel Method for Motions and Loads of Ships with Forward Speed." *Schiffstechnik (Ship Technology Research)*, Volume 39, pp. 147-156, 1992.

Payne, A. and R. Issa. *Grasshopper Primer for Version 0.6.0007*, 2009.

Salvesen, N., E.O. Tuck and O. Faltinsen. "Ship Motions and Sea Loads." *Transactions, Society of Naval Architects and Marine Engineers*, Volume 78, 1970.

Schellin, T.E., X.-B. Chen, C. Beiersdorf and A. Maron. "Comparative Frequency Domain Seakeeping Analysis of a Fast Monohull in Regular Head Waves." *21st International Conference on Offshore Mechanics and Arctic Engineering*, Oslo, 2002.

Stern, F., J. Yang, Z.Wang, H. Sadat-Hosseini, M. Mousaviraad, S. Bhushan and T. Xing. "Computational Ship Hydrodynamics: Nowadays and Way Forward." *International Shipbuilding Progress*, Volume 60, pp. 3-105, 2013.

Telste, J.G. and F. Noblesse, "Numerical Evaluation of the Green Function of Water-Wave Radiation and Diffraction." *Journal of Ship Research*, Volume 30, Number 2, 1986.

Wang, E., Q. Zhang, B. Shen, G. Zhang, X. Lu, Q. Wu and Y. Wang. *High-Performance Computing on the Intel®Xeon Phi™*, Springer International Publishing, Switzerland, 2014.

Wehausen, J.V. "The Motion of Floating Bodies." *Annual Review of Fluid Mechanics*, Volume 3, pp. 237-268, 1971.